

High-Performance Supercapacitor Electrodes Based on Porosity-Controllable Carbon Paper by Centrifugal Spinning

Boshi Ji,^[a] Zhiyu Wu,^[a] Jun Hu,^[a, b] Chen Huang,^[b] Pei Lyu,^{*[a, c]} Heng Pan,^[a] Jie Ren,^[a] Bin Shang,^[a, b] and Xin Liu^{*[a, b]}

Carbon paper is widely utilized in supercapacitors primarily for its notable attributes, including high specific surface area, commendable electrical conductivity, and excellent chemical stability. Then investigate the effect of carbon paper with different porosities as supercapacitor substrates on the electrochemical performance of electrodes. Meanwhile, tungsten oxide is grown on the surface of carbon paper using the hydrothermal method to test the electrochemical performance of the composite electrode. The prepared carbon paper and oxygen-deficient tungsten oxide (WO_x) composite electrode (CP@WO_x) exhibit an area-specific capacitance of 915.8 mF/cm² at a current density of 5 mA/cm². In addition, the electrode exhibits

good cycling stability. After 20,000 cycles, the capacitance remains 104.1% of the original capacity at 50 mA/cm² current density. Solid-state symmetric supercapacitors assembled using CP@WO_x electrode exhibit excellent performance in terms of surface energy density of 6.25 µWh/cm² (at a power density of 0.6 mW/cm²) and maintain 100.4% of their original capacity after 7000 charge/discharge cycles. Relying on the higher productivity advantage of centrifugal spinning technology over electrostatic spinning technology and other preparation processes, this study develops a new way of thinking for the large-scale production of composite electrode materials, which has more considerable potential for large-scale development.

1. Introduction

The rapid development of the global economy and global warming urgently require the development of new green and efficient energy devices to solve energy and environmental problems. The new energy sources represented by wind, hydrogen, and solar energy are often influenced by environmental factors, resulting in unstable power generation and cannot be used anywhere. A variety of types of energy storage devices are needed to convert new energy sources into electricity for storage and transportation.^[1] At present, the main common energy storage devices are batteries and supercapacitors. Batteries have high energy density but short cycle life, and supercapacitors have high power density and excellent cycle stability but lower energy density.^[2-9] To overcome the low energy density of ultracapacitors, there is an urgent need to develop solutions with higher energy density. Batteries and

ultracapacitors are often used in combination to improve overall system efficiency through synergistic effects.

Energy storage devices usually need to transfer and store charges quickly, operate stably for a long period of time, and maintain low cost. Carbon materials are widely used in the field of energy storage materials due to their good electrical conductivity, excellent chemical stability, and simple preparation.^[10,11] As a form of carbon material, carbon paper is lightweight and has good structural stability, which makes it an indispensable part of electrode materials.^[12,13] Composite electrodes are usually prepared by attaching active substances to the surface of carbon paper, which can significantly enhance the performance of supercapacitors. The structure of carbon fibers in carbon paper exerts a significant influence on the performance of electrodes. Among them, the thickness of the carbon fibers and the porosity of the three-dimensional structure affect the specific surface area of the carbon paper, while the overall density of the carbon paper affects the electrical conductivity of the carbon paper, which in turn has a great impact on the performance of the electrode. However, the current research puts more attention on the active substance aspect and neglects to perfect the electrode substrate. The current research on carbon paper collectors is still insufficient and lacks a simple and effective method to flexibly control the porosity and density of carbon paper. Further tuning of the three-dimensional structure of carbon paper would help optimize the size and energy storage performance of supercapacitors.

Centrifugal spinning is a technique that produces micro-to-nanometer fibers. Fibers prepared by centrifugal spinning have been used in various fields such as photocatalysis,

[a] B. Ji, Z. Wu, J. Hu, P. Lyu, H. Pan, J. Ren, B. Shang, X. Liu
State Key Laboratory of New Textile Materials & Advanced Processing Technology, Wuhan Textile University, Wuhan 430073, P. R. China
E-mail: peilyu@wtu.edu.cn
xinliu@wtu.edu.cn

[b] J. Hu, C. Huang, B. Shang, X. Liu
School of Materials Science and Engineering, Wuhan Textile University, Wuhan 430200, P. R. China

[c] P. Lyu
School of Textile Science and Engineering, Wuhan Textile University, Wuhan 430200, P. R. China

 Supporting information for this article is available on the WWW under <https://doi.org/10.1002/batt.202400559>

biomedicine, energy storage, and filtration.^[14] During centrifugal spinning, centrifugal force compels polymer jets to form threadlets and further into fibers. The high productivity and controllable fiber structure enable it to be used as an important technique for the preparation of carbon papers.^[15] Transition metal oxides, such as RuO₂,^[16] and ZnO,^[17] are widely employed as active materials for energy storage devices. However, the low conductivity of metal oxides makes them unsuitable for energy storage applications. To enhance the overall electrochemical performance of electrodes, it is possible to prepare composite electrodes by combining them with carbon materials. W₁₈O₄₉ is renowned for its superior electrochemical properties. Monoclinic W₁₈O₄₉ contains tungsten in the W⁵⁺ oxidation state and the presence of oxygen vacancies reduces the resistivity of oxide materials, thereby facilitating good electrochemical activity.^[18] Furthermore, by designing nanoscale structures of metal oxides, the conductivity and ion transfer efficiency of materials can be increased, thus optimizing the performance of supercapacitors.

Fu^[19] et al. fabricated uniform and ultrathin carbon paper by assembling highly flat, few-walled carbon nanotubes (FWCNTs) and short carbon fibers by mixing pumping, and filtering. However, the shortcoming is that the density and porosity of carbon paper cannot be flexibly controlled, and the structure of carbon paper cannot be further regulated. Sun^[20] et al. prepared lightweight, low-cost carbon paper by simple electrostatic spinning and annealing and used it in friction nanogenerators. However, electrostatic spinning has the defects of low yield, and the resulting fiber mats are tightly connected, which makes it difficult to adjust their three-dimensional structure. In contrast, centrifugal spinning technology presents a fluffy fiber on the collection plane through high-speed spinning, which allows flexible adjustment of the three-dimensional structure of the fiber mats during the hot-pressing process. Our work focuses on optimizing the carbon paper preparation process to enhance the performance of electrode materials by adjusting the density of carbon paper to affect its conductivity and porosity. This research direction is different from the previous ones, focusing on improving the properties of the carbon paper itself, which lays the foundation for optimizing the performance of the composite electrodes.

In this study, we propose a novel method for manufacturing carbon paper (CP) collectors with adjustable density and conductivity. These collectors are subsequently used in the production of high-performance supercapacitors by combining them with WO_x. At the same time, we purchased TGP-H-060 (TCP) model carbon paper from Toray, Japan for comparison, and the results indicated that the carbon paper prepared in this study exhibited better electrochemical properties. The resulting CP@WO_x composite electrode exhibited a high specific capacitance of 915.8 mF/cm² at a current density of 5 mA/cm². To verify their practicality, we assembled symmetric supercapacitors using these CP@WO_x composite electrodes, thereby presenting a scalable production method for supercapacitors.

Experiment

Materials

Polyacrylonitrile (PAN) powder (average molecular weight:150000), and tungsten chloride powder (99.9% metals basis) were supplied by Shanghai Macklin Biochemical Technology Co., Ltd. (Shanghai, China). N, N-dimethylformamide (DMF, anhydrous, ≥99.5%) was purchased from Sinopharm Chemical Reagent Co., Ltd. (Shanghai, China).

Centrifugal Spinning for Carbon Paper Preparation

Figure 1a shows a schematic diagram of fabricating PAN fiber mats using centrifugal spinning technology. A negative pressure space was provided underneath the fiber mats to allow a planar collection of fibers. A high production rate was achieved by setting the spinning speed at 4500 r/min.

PAN powder with a molecular weight of 150,000 was dissolved in DMF to form a spinning solution with a PAN content of 25%, followed by vacuum defoaming. During the centrifugal spinning process, the ambient temperature was maintained at approximately 40 °C, the fiber collection height was 4 cm, the orifice size of the spinneret was 0.16 mm, and the ambient humidity was maintained at 30–50%.

After the preparation of polyacrylonitrile fiber mats using the planar centrifugal spinning technique, PAN fiber papers with different densities and porosities were obtained after different hot pressing (4 MPa, 6 MPa, 8 MPa, and 10 MPa, hereinafter referred to as CP-4, CP-6, CP-8, and CP-10, respectively) treatments. Finally, CP was obtained after pre-oxidation at 280 °C and carbonization at 1000 °C.

Composite Electrode Preparation

A hydrothermal solution was formed by dissolving 200 mg of tungsten hexachloride powder in 50 ml of anhydrous ethanol through continuous stirring for 30 minutes. The carbon paper was sequentially immersed in acetone and anhydrous ethanol for ultrasonic cleaning, followed by repeated washing with deionized water and plasma treatment for 200 seconds. The hydrothermal solution was injected into a polytetrafluoroethylene reactor. Subsequently carbon paper cut to 1×2 cm was placed in the growth solution, and the growth was carried out under hydrothermal conditions at 180 °C for 600 min. After removal, it was dried at 60 °C for 6 hours to obtain the CP@WO_x composite electrode.

Fabrication of Symmetrical Supercapacitor Devices

To validate the electrodes with the same mass, the same area of two electrode plates with polyvinyl alcohol (PVA)-H₂SO₄ gel electrolyte placed in the middle were used. Firstly, 3 g of PVA powder was dissolved in 30 ml of deionized water and stirred at 90 °C for one hour. Then 3 g of concentrated sulfuric acid at 98% concentration was added under shaking until the turbidity became clear. After evaporating the excess water under vacuum, the gel electrolyte was placed between two electrodes.

A polydimethylsiloxane (PDMS) solution was prepared by mixing the prepolymer gel (Sylgard 184 Silicone Elastomer Base) and the cross-linking agent (Sylgard 184 Silicone Elastomer Curing Agent). Subsequently, the PDMS solution was applied to the outer surfaces of the two electrodes and the device was sealed. After vacuum drying for 12 hours, the symmetric supercapacitor device was obtained.

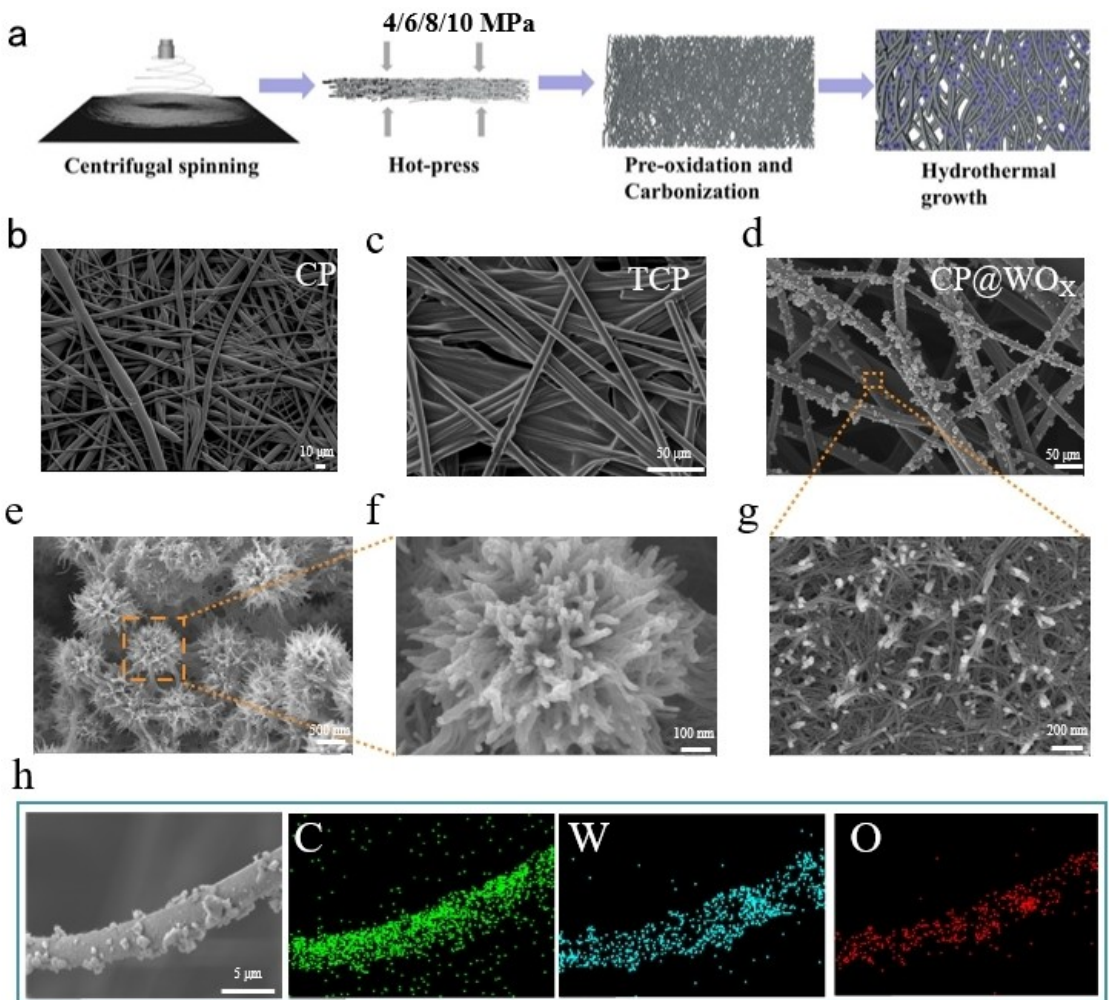


Figure 1. (a) Schematic diagram of electrode fabrication, (b) SEM image of CP, (c) SEM image of TCP, (d) SEM image of WO_x nanorods attached to the surface of carbon fibers, (e-f) SEM image of WO_x nanorods, (g) SEM image of WO_x nanowires, and (h) EDS mappings of C, W, and O.

Electrochemical Measurements

To characterize the electrochemical properties of the prepared $\text{CP}@\text{WO}_x$, a CHI-760 E electrochemical workstation equipped with a standard three-electrode system was used to perform cyclic voltammetry (CV), galvanostatic charge-discharge (GCD) and Electrochemical Impedance Spectroscopy (EIS). We utilized a three-electrode system to evaluate the performance of the $\text{CP}@\text{WO}_x$ electrode, which was fabricated in advance, at room temperature. The chosen electrolyte solution was 1 M H_2SO_4 . The operating potential range was set from -0.5 V to 0.1 V. In this configuration, the $\text{CP}@\text{WO}_x$ functioned as the working electrode, while the Pt sheet and Ag/AgCl electrodes were used as the counter and reference electrodes, respectively. For the examination of the cycling stability of individual electrodes, a current density of 50 mA/cm 2 was applied for a total of 20,000 cycles. To assess the cycling stability, we compared the average discharge time obtained every five hundred cycles. As for the supercapacitor device, the cycling stability was evaluated by subjecting it to 7000 cycles with a current density of 30 mA/cm 2 . The average discharge time over two hundred cycles was used to establish the cycle stability.

The area-specific capacitance of the electrodes (C_a , expressed as mF/cm 2), the area energy density (E , expressed as $\mu\text{Wh}/\text{cm}^2$), and the area power density (P , expressed as mW/cm 2) of the super-

capacitor can be calculated according to the following equations^[21–23]:

$$C_a = I\Delta t/\Delta V \quad (1)$$

$$E = C_a \times \Delta V^2 / 2 \times 3.6 \quad (2)$$

$$P = C_a \times \Delta V^2 / 2 \times 3.6 \quad (3)$$

Where I and Δt are the discharge current (mA) and discharge time (s) of the GCD test, A is the electrode effective area (cm 2), and ΔV is the voltage window (V).

Characterizations

The surface micromorphology of carbon paper and tungsten oxide nanorods was observed by scanning electron microscope (SEM, JSM-7800, JEOL, Japan and Gemini SEM 300, Germany) at an accelerating voltage of 5.0 kV, respectively. The structure and composition of the samples were examined using a confocal micro-Raman imager (labRAM Odyssey, HORIBA Lab RAM Odyssey, France), an X-ray diffractometer (X'pert PRO, PAN analytical, The Netherlands), and an X-ray photoelectron spectrometer (XPS,

Thermo Scientific K-Alpha, USA). The conductivity and resistivity of PFP were measured using a dual electrometric four-point probe tester (RTS-9, Guangzhou 4 PROBES TECH, China).

2. Results and Discussion

Figure 1a shows the preparation process of CP@WO_x, which includes centrifugal spinning to prepare polyacrylonitrile-based fiber membranes, polyacrylonitrile fiber paper obtained after treatment with different hot-pressing pressures, further pre-oxidation and carbonization to obtain CP, and finally hydrothermal reaction to attach WO_x nanospheres on the surface of carbon paper. CP, TCP, and CP were compared after loading WO_x to exhibit the morphology differences among the electrode materials. As shown in Figure 1b, the carbon paper prepared by centrifugal spinning (CP) exhibited a dense three-dimensional mesh structure. As the amount of fiber per unit volume increased in CP due to the dense structure. Figure 1c shows the SEM image of TCP, the surface of carbon fiber in TCP is rough (Figure S1b). The surface of carbon fiber in CP is smooth (Figure S1a). Besides, CP exhibited a smaller average diameter compared with TCP (Figure S2), which further increased the specific surface area. This made CP promising candidates as supercapacitor fluid collectors which could attach more active materials.

The surface of the carbon fibers after hydrothermal growth was characterized by the distribution of sea urchin-like WO_x nanorods (Figure 1d). Each nanosphere was composed of a large number of nanowires, forming a three-dimensional structure. The cluster structure increased the specific surface area and provided more electrochemically active sites (Figure 1e and f). Similarly, WO_x exists in the same form on the surface of TCP fibers (Figure S1c,d). Where nanospheres did not

form on the carbon fiber surface, WO_x nanowires exist in the form of Vine-like and are tightly wound around the carbon fiber surface (Figure 1g). This structure was stable and favored the stability of the material, and the pores in the middle of the nanowires provided convenient channels for the embedding and dislodging of ions. Figure 1h demonstrates the EDS-Mapping image of CP@WO_x, which clearly shows the uniform distribution of carbon (C), oxygen (O), and tungsten (W) elements on the corresponding nanofibers.

To analyze the structure and composition of the prepared samples, we conducted Raman spectroscopy, X-ray diffraction analysis (XRD), and X-ray photoelectron spectroscopy (XPS).

The phases of WO_x were distinguished by the Raman technique as shown in Figure 2a. There were three main signal peaks that appeared at 255 cm⁻¹, 697 cm⁻¹, and 805 cm⁻¹. In the W₁₈O₄₉ crystal structure, 255 cm⁻¹ belongs to the O–W–O bending mode. The peaks at 697 cm⁻¹ and 805 cm⁻¹ can be attributed to the W–O stretching mode.^[24] Due to the long length of W–O–W bond lengths in the structure of W₁₈O₄₉, the broad bands at 697 cm⁻¹ and 805 cm⁻¹ are broader. This can be attributed to the oxidation state of tungsten atoms in the low-valent oxides of tungsten from W⁴⁺ to W⁶⁺.

Figure 2b shows the Raman spectrum of CP, where the G band is located at 1587 cm⁻¹, while the D band is located at 1355 cm⁻¹. The ratio of the D band to the G band (ID/IG) was 1.24, which indicated the presence of considerable amorphous structure and structural defects in the material, which could provide more active sites to improve the performance when acting as supercapacitor electrodes.^[25]

Figure 2c shows the XRD curves of CP, WO_x, and CP@WO_x. After the pre-oxidation and carbonization treatments, CP showed a strong diffraction peak at $2\theta=25^\circ$, representing the diffraction peak of the (002) crystal plane.^[26] In addition, a weak diffraction peak at $2\theta=44^\circ$, representing the diffraction peak of

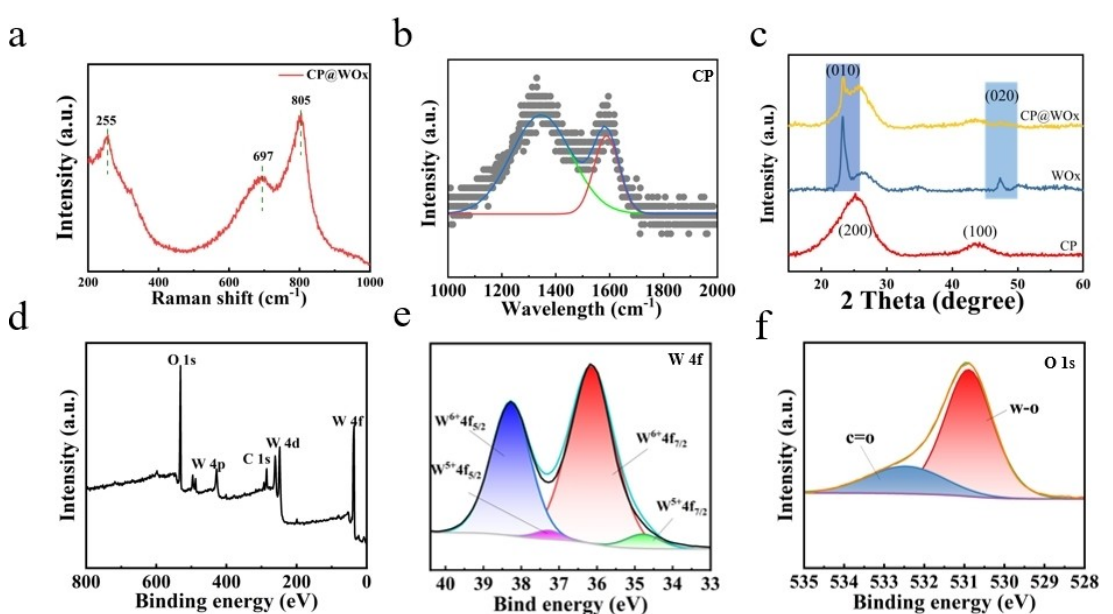


Figure 2. Raman images of (a) CP@WO_x, (b) CP; (c) XRD images of CP, WO_x, and CP@WO_x; (d) XPS analysis of CP@WO_x; High-resolution spectra of (e) W4f and (f) O1s of CP@WO_x.

the crystal plane (100), was observed. This indicated that the two-dimensional vortex-layered graphite planar structure in the carbon fibers was gradually transformed into a three-dimensional ordered structure during the carbonization process, forming a graphite crystal-like structure. The crystalline phase and crystallinity of the $W_{18}O_{49}$ nanostructures were characterized using XRD. Comparison with a standard chart card (JCPDS 71–2450) indicates that the prepared product is a pure monoclinic $W_{18}O_{49}$. The two strong diffraction peaks at 23.35° and 47.25° correspond to the (010) and (020) crystal planes of the monoclinic crystal system, which denoted the anisotropic growth of $W_{18}O_{49}$.^[27,28]

In order to further confirm the chemical composition and valence of the micro-nanospheres on CP@WO_x, XPS tests were performed (Figure 2d). The high-resolution spectrum of the W 4f core energy level was shown in Figure 2e. There were two main peaks at 36.1 and 38.2 eV, which could be attributed to the W⁶⁺ 4f_{7/2} and W⁶⁺ 4f_{5/2} binding energies, indicating the presence of W⁶⁺ in the sample. The peaks located at 37.2 eV and 34.8 eV corresponded to W⁵⁺ 4f_{5/2} and W⁵⁺ 4f_{7/2}. This indicated the presence of low-valence W⁵⁺ in the resulting tungsten oxide, suggesting the presence of free oxygen vacancies in the tungsten oxide prepared by the hydrothermal method.^[29] The presence of oxygen vacancies was further determined by the O 1s core energy level spectra (Figure 2f). The peak located at 530.9 eV corresponded to the W–O–W oxygen bond, while the peak located at 532.5 eV could be

attributed to the O atoms close to the oxygen vacancies. This result further confirmed the existence of oxygen vacancies in WO_x, which provided additional active sites.^[27]

As shown in Figure 3a, with the increase of hot-pressing strength, the thickness of fiber mats decreased while the density increased. This was because the fibers were more compact to each other, and the structure got more stable. The conductivity of carbon paper increased with the increase of hot-pressing strength, but the porosity decreased (Figure 3b). As a substrate for supercapacitor fluid collectors, it should have high electrical conductivity for electron transfer, and it needs to have appropriate porosity to achieve a large specific surface area for electrolyte penetration, diffusion, and high active substance loading. As shown in Figure 3c, the pore distribution of carbon paper was measured by the mercury-pressed meter. With the increase in pressure, the overall pore size and content of carbon paper showed a decreasing trend. Detailed values are shown in Table 1. In Figure 3d, the surface SEM images of carbon paper treated with different hot-pressing strengths were demonstrated. It could be observed that with the increase in pressure, more fibers were presented per unit area. The gap between fibers decreased, as marked in yellow and the structure of carbon paper tended to be dense. Due to compression, more fibers appeared on the surface, and the effective specific surface area of the carbon paper decreased. Even though compressing could give a compact and stable structure, the decreased specific surface area was not conducive

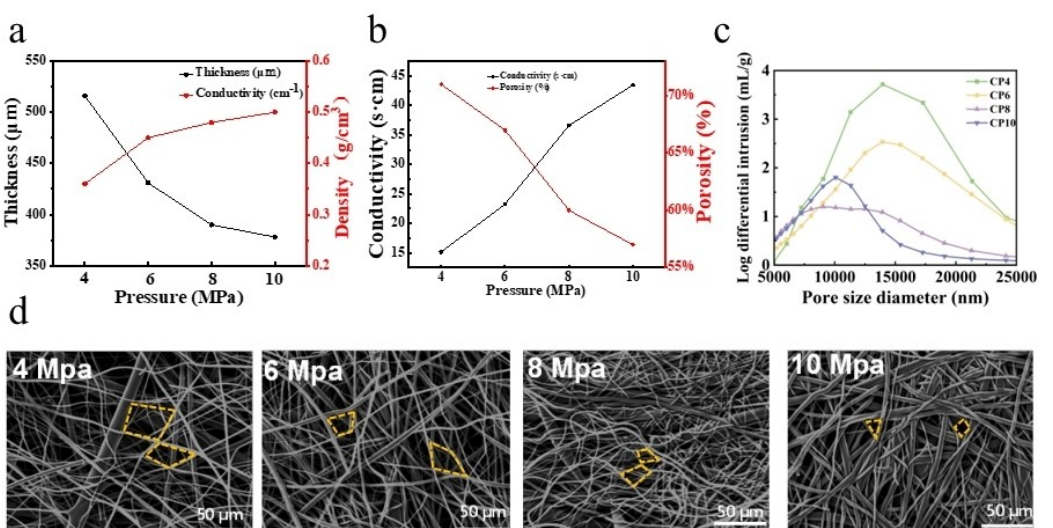


Figure 3. Carbon paper after 4, 6, 8, and 10 MPa hot-pressing treatment, (a) thickness vs. density, (b) electrical conductivity vs. porosity, (c) pore distribution, (d) SEM images.

Table 1. Parameters of carbon paper after different hot-pressing strengths.

	Hot-pressing pressure (MPa)	Thickness (μm)	Density (g/cm³)	Porosity (%)	Area-specific capacitance (mF/cm²)
CP@WO _x -4	4	516	0.36	0.71	790.8
CP@WO _x -6	6	431	0.45	0.67	915.8
CP@WO _x -8	8	390	0.48	0.60	799.2
CP@WO _x -10	10	378	0.5	0.57	680.8

to the attachment of active substances and might affect the ion transport rate. Thus, an optimum compressing strength needed to be explored to balance stable fiber structure and good electrochemical performance.

Cyclic Voltammetry was used to investigate the electrochemical reaction behavior at the interface between the carbon paper-based electrode and the electrolyte. CP, TCP, and CP@WO_x were tested at a scan rate of 50 mV/s. As shown in Figure 4a, CP and CP-Toray did not undergo redox reactions for charge collection.

The peak current and integration area of CP@WO_x-6 increased significantly with increasing scan rate (Figure 4b), indicating fast charge transfer and ion insertion/detachment properties. The contours of the CV curves were clearly different from the typical rectangular shape of an electric double-layer capacitor, showing the pseudocapacitive properties of CP@WO_x-6. With the increase in scan rate, the peak current and the integration area of CP@WO_x-6 increase significantly, indicating the fast charge transfer and ion insertion/detachment characteristics. Meanwhile, the contours of the CV curves could be maintained at low scan rates and a pair of redox peaks could be observed, showing good reversibility. As the scan rate increased, the positions of the anodic and cathodic peaks moved to higher and lower potentials, respectively, showing a fast current response of the material.

As shown in Figure 4c, the composite electrodes of CP and TCP after hydrothermal growth of tungsten oxide at different pressure treatments were tested at a scan rate of 50 mV/s. Although CP10 exhibited improved electrical conductivity with increasing hot compression strength, its electrochemical performance was not optimal. Notably, CP@WO_x-6 still exhibited a larger area compared to TCP@WO_x, which was attributed to its balanced porosity, conductivity, and carbon paper pore size. The larger carbon paper porosity helps provide more electrochemically active sites and a wider space for tungsten oxide attachment and facilitates ion diffusion. Figure S3 shows the CV curves of TCP@WO_x, CP@WO_x-4, CP@WO_x-8, and CP@WO_x-10 at different scan rates.

In order to distinguish the type of energy storage of the obtained electrode materials, we analyzed the relative contribution of surface control and diffusion control to the charge storage process (Figure 4d). We obtained quantitative charge storage by analyzing the peak current (*i*) and scan rate (*v*) of the CV curves using a method based on the equation:

$$i = av^b \quad (4)$$

Where *a* and *b* were adjustable parameters, the measured current *i* obeyed a power-law relationship with the scan rate *v*; *a* and *b* were variables. In particular, the *b*-value of 0.5 indicates

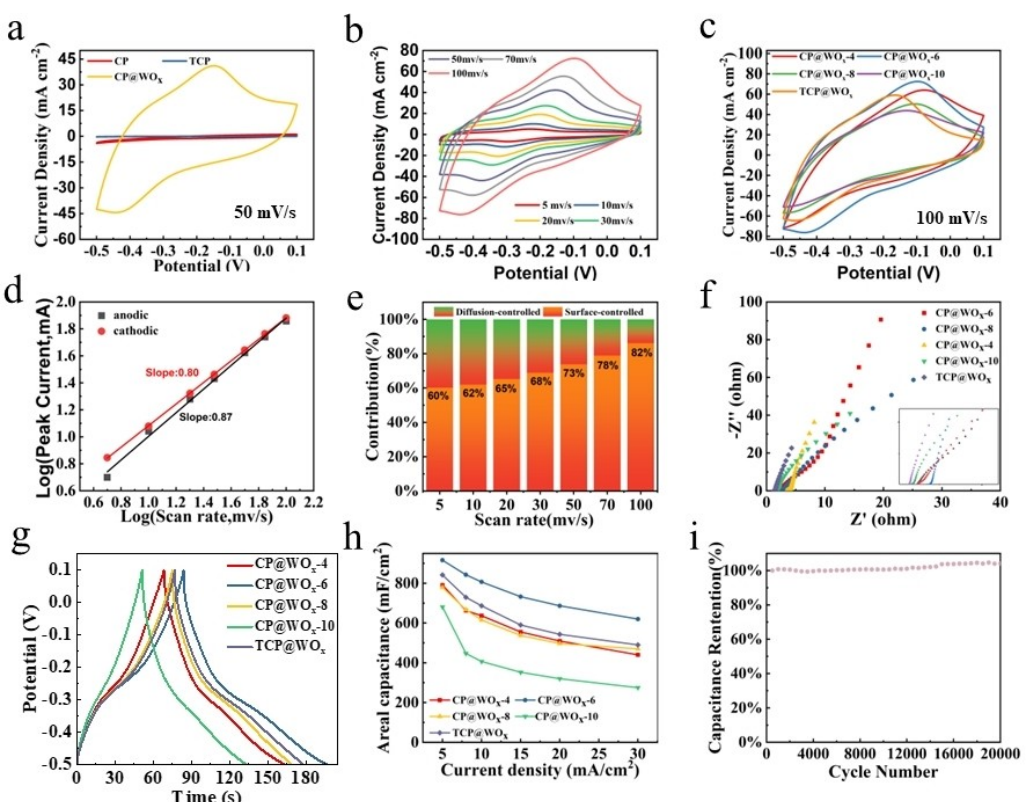


Figure 4. (a) CV curves of CP, TCP, and CP@WO_x-6 at a scan rate of 50 mV/s, (b) CV curves of CP@WO_x-6 at different voltage scan rates, (c) CV curves of different electrodes at a scan rate of 100 mV/s, (d) Relationship between the peak current of the CP@WO_x-6 electrode and the scan rate, (e) Ratio of capacitance control to diffusion control during the electrochemical reaction at different scan rates, (f) EIS analysis of electrodes in 1 M H₂SO₄ electrolyte, (g) EIS analysis of electrodes in 1 M H₂SO₄ electrolyte, (h) CV curves of different electrodes at 100 mV/s scan rate, (e) Ratio of capacitance control to diffusion control during electrochemical reaction at different scan rates, (f) EIS analysis of electrodes in 1 M H₂SO₄ electrolyte, (g) GCD curves of different electrodes at 5 mA/cm², (h) Area-specific capacitance of different samples at different current densities, (i) Cycling stability of CP@WO_x-6 electrode at 50 mA/cm².

a diffusion-controlled process, whereas 1.0 represents a surface-controlled process. To confirm the mechanism of charge storage, we plotted the log (i) versus log (v) curves of the anodic and cathodic peaks in the range of 5 to 100 mV/s. The calculated b values for the cathodic and anodic peaks of CP@WO_x-6 were 0.80 and 0.87, respectively. Since these b values were close to 1.0, it could be assumed that the charge storage process was diffusion-independent, thus exhibiting excellent rate capability.

The accuracy of quantitatively analyzing the ratio of diffusion-controlled and surface-controlled processes could be improved by this equation:

$$i = k_1 v + k_2 v^{\frac{1}{2}} \quad (5)$$

Where k_1 and k_2 were constants that could be obtained from the CV curves at different scanning rates. The proportion of diffusion control decreases with increasing sweep speed. This is mainly due to the fact that at lower sweep speeds, the WO_x nanospheres in CP@WO_x are in full contact with the electrolyte solution and undergo sufficient electrochemical reactions.^[30,31]

Electrochemical impedance analysis provided a deep understanding of the performance and kinetic behavior of electrochemical morphology and provided us with important information about the electrode-electrolyte interface and the overall system kinetic properties. We performed electrochemical impedance spectroscopy (EIS) in the frequency range of 0.01 Hz-100 kHz, as shown in Figure 4f. The inset showed the detailed high-frequency response. As the hot-pressing intensity increased, the equivalent series resistance (ESR) of the composite electrode showed a gradual decrease. The specific ESR values recorded for CP@WO_x-4, CP@WO_x-6, CP@WO_x-8, CP@WO_x-10, and TCP@WO_x were 3.14, 2.28, 2.05, 1.57, and 1.23, respectively. The progressively declining ESR signified a tendency for the internal fiber structure of the carbon paper current collector to compact, resulting in improved conductivity.

The GCD curves of different electrodes were illustrated in Figure 4g for a current density of 5 mA/cm². It was evident from the figure that CP@WO_x-6 demonstrated the highest energy storage capacity. Figure S4 shows the GCD curves of TCP@WO_x (a), CP@WO_x-4 (b), CP@WO_x-6 (c), CP@WO_x-8 (d), and CP@WO_x-10 (e) at different current densities. The comparative results of the area-specific capacitance of different electrodes at a current density of 5 mA/cm², as calculated from the GCD curves, were presented in Figure 4h. The descending order of the area-specific capacitance for each electrode was as follows: CP@WO_x-6 (915.8 mF/cm²), TCP@WO_x (841.7 mF/cm²), CP@WO_x-4 (790.8 mF/cm²), CP@WO_x-8 (779.2 mF/cm²), and CP@WO_x-10 (680.8 mF/cm²).

Cycling stability is a crucial characteristic of supercapacitors. To assess the cycling stability, we conducted 20,000 charge/discharge tests. Remarkably, even after undergoing 20,000 cycles, the supercapacitor retained its capacity at 104.1% of the original value (Figure 4i), signifying excellent stability. Throughout the continuous charge and discharge process, the active materials within the electrodes gradually activated, resulting in an increased electrode capacity.

In order to evaluate the practical performance of the prepared CP@WO_x electrode, we prepared symmetric supercapacitors using this electrode. Figure 5a showed that the CV curves were almost identical at different scan rates. Figure 5b shows the GCD curves of this symmetric supercapacitor at different current densities. According to the calculation, this symmetric supercapacitor exhibited a specific capacitance of 125 mF/cm² at a current density of 2 mA/cm². The cycle stability of the symmetric supercapacitor was tested after a 7000-cycle charging and discharging test. The capacity was still maintained at 100.4% of the original capacity after 7000 cycles, which indicated good stability. Based on the obtained GCD curve data, Figure 5d shows the Lagoon plot of area energy density and power density. The energy density of this symmetric supercapacitor device was 6.25 µWh/cm² at a power density of 0.6 mW/cm². As presented in Figure 5d and Table 2, the supercapacitors prepared in this study exhibit superior performance compared to other material supercapacitors.^[32-39]

3. Conclusions

Carbon paper with controlled porosity was prepared by centrifugal spinning. Oxygen-deficient tungsten oxide was combined with carbon paper to form a supercapacitor electrode. The composite electrode exhibited a capacitance of 951.8 mF/cm² at a current density of 5 mA/cm². After undergoing 20,000 cycles, the electrode maintained 104.1% of its original capacity. The symmetric supercapacitor device assembled from this electrode achieved an energy density of 6.25 µWh/cm² at a power density of 0.6 mW/cm². The device retained 100.4% of its initial capacity after 7,000 cycles of testing, demonstrating excellent cycling stability. By simply manipulating the carbon paper's density and porosity, we have optimized the specific capacitance of the composite electrode when used as a current collector. The scalability of the centrifugal spinning technology suggests that it has the potential to produce carbon paper continuously, providing a new approach to the large-scale manufacture of supercapacitor electrodes.

Table 2. parameters of carbon paper after different hot-pressing strengths.

	This work	[32]	[33]	[34]	[35]	[36]	[37]	[38]	[39]
Power density (µW/cm ²)	600.0	24.5	204.8	387.5	50.0	410.0	109.0	119.0	25.0
Energy density (µWh/cm ²)	6.25	1.24	1.7	1.8	5.8	5.8	2.6	3.6	5.9

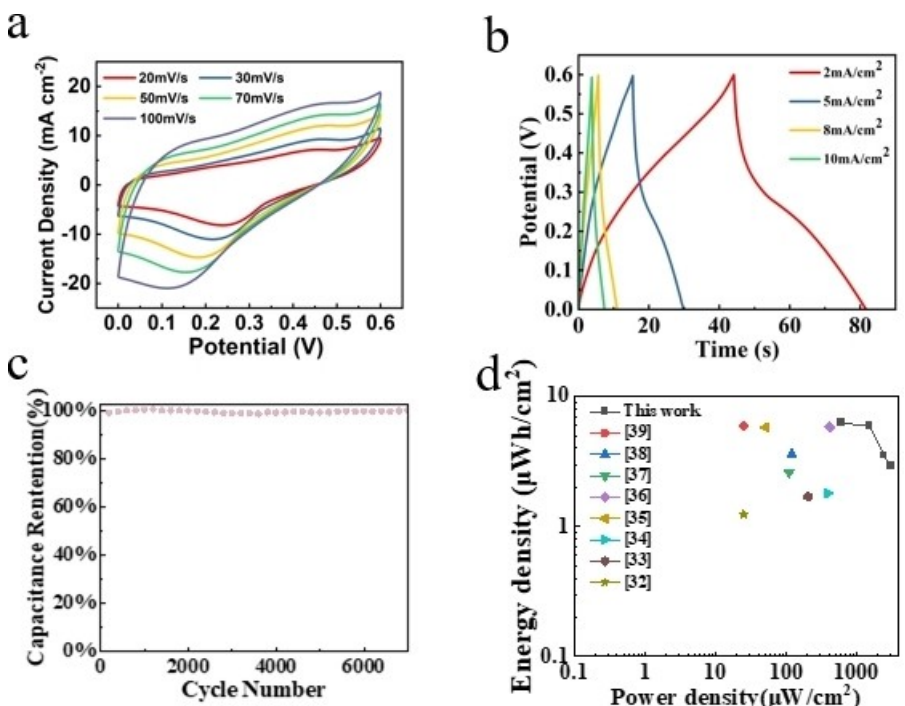


Figure 5. (a) Electrochemical testing of a symmetric supercapacitor, (a) CV curves at different sweep rates, (b) GCD curves at different current densities, (c) Cycling stability testing of this supercapacitor in the 0–0.6 V range, (d) Lagoon plots of energy density and power density of the device at different charging and discharging rates.

Acknowledgements

Thanks to the Analysis and Testing Center of Wuhan Textile University for providing the characterization instruments. This work was supported by the National Natural Science Foundation of China (No. 52173062, U21A2095), the Key Research and Development Program of Hubei Province (No. 2020BAB080, 2021BAA068), the open project of the State Key Laboratory of New Textile Materials and Advanced Processing Technologies (FZ20230022).

Conflict of Interests

The authors declare no conflict of interest.

Data Availability Statement

The data that support the findings of this study are available from the corresponding author upon reasonable request.

Keywords: Centrifugal spinning • Carbon paper • Composite electrodes • Supercapacitors • Porosity

- [1] M. Jalalah, H. Han, A. K. Nayak, F. A. Harraz, *Adv. Compos. Hybrid Mater.* **2024**, 7(1), 20.
- [2] H. Li, R. Chen, M. Ali, H. Lee, M. J. Ko, *Adv. Funct. Mater.* **2020**, 30(47), 2002739.
- [3] Z. Guo, X. Han, C. Zhang, S. He, K. Liu, J. Hu, W. Yang, S. Jian, S. Jiang, G. Duan, *Chin. Chem. Lett.* **2024**, 35(7), 109007.
- [4] J. Yang, Y. Wang, Y. Liu, G. Duan, Z. Liang, J. Han, Y. Huang, X. Han, C. Zhang, S. He, S. Jiang, *Fuel* **2025**, 379, 133048.
- [5] Y. Huang, L. Xing, S. Pei, W. Zhou, Y. Hu, W. Deng, L. Chen, H. Zhu, H. Chen, *Trans. Nonferrous Met. Soc. China* **2023**, 33(11), 3452–3464.
- [6] Y. Liu, K. Xiang, W. Zhou, W. Deng, H. Zhu, H. Chen, *Small* **2024**, 20(20), 2308741.
- [7] S. Zeng, G. Duan, R. Yu, Q. Qin, S. He, S. Jiang, H. Yang, X. Han, J. Han, B. Y. Xia, *Prog. Mater Sci.* **2025**, 147, 101356.
- [8] S. Jiang, H. Liu, W. Zhang, Y. Lu, *Bioresour. Technol.* **2024**, 405, 130936.
- [9] L. Li, J. S. Nam, M. S. Kim, Y. Wang, S. Jiang, H. Hou, I.-D. Kim, *Adv. Energy Mater.* **2023**, 13(36), 2302139.
- [10] Z. Tian, C. Yang, C. Zhang, X. Han, J. Han, K. Liu, S. He, G. Duan, S. Jian, J. Hu, W. Yang, S. Jiang, *J. Energy Storage* **2024**, 85, 111130.
- [11] Z. Tian, G. Duan, F. Wang, Y. Wang, H. Hou, C. Zhang, S. He, J. Han, X. Han, S. Jiang, *Chem. Eng. J.* **2024**, 484, 149615.
- [12] W. Xu, D. Du, R. Lan, J. Humphreys, D. N. Miller, M. Walker, Z. Wu, J. T. S. Irvine, S. Tao, *Appl. Catal. B-Environ.* **2018**, 237, 1101–1109.
- [13] Y. K. Lee, K. Y. Cho, S. Lee, J. Choi, G. Lee, H. I. John, K. Eom, S. Lee, *Adv. Energy Mater.* **2023**, 13(9), 2203770.
- [14] B. N. Tepekiran, M. D. Calisir, Y. Polat, Y. Akgul, A. Kilic, *Aerosol Sci. Technol.* **2019**, 53(8), 921–932.
- [15] J. Ayala, D. Ramirez, J. C. Myers, T. P. Lodge, J. Parsons, M. Alcoutabi, *J. Mater. Sci.* **2021**, 56(28), 16010–16027.
- [16] K. Brousse, S. Pinnaud, S. Nguyen, P. F. Fazzini, R. Makarem, C. Josse, Y. Thimonet, B. Chaudret, P. L. Taberna, M. Respaud, P. Simon, *Adv. Energy Mater.* **2020**, 10(6), 1903136.
- [17] L. Xu, C. Huang, Z. Hua, L. Chen, *Energy Storage Mater.* **2023**, 61, 102888.
- [18] M. R. Thalji, G. A. M. Ali, P. Liu, Y. L. Zhong, K. F. Chong, *Chem. Eng. J.* **2021**, 409, 128216.
- [19] X. Fu, J. Wei, F. Ning, C. Bai, Q. Wen, H. Jin, Y. Li, S. Zou, S. Pan, J. Chen, S. Deng, X. Zhou, *J. Power Sources* **2022**, 520, 230832.
- [20] N. Sun, Z. Wen, F. Zhao, Y. Yang, H. Shao, C. Zhou, Q. Shen, K. Feng, M. Peng, Y. Li, X. Sun, *Nano Energy* **2017**, 38, 210–217.
- [21] X. Dong, H. Jin, R. Wang, J. Zhang, X. Feng, C. Yan, S. Chen, S. Wang, J. Wang, J. Lu, *Adv. Energy Mater.* **2018**, 8(11), 1702695.
- [22] S. Zhang, N. Pan, *Adv. Energy Mater.* **2015**, 5(6), 1401401.

- [23] M. Lai, K. Chen, D. Wang, P. Cai, L. Sun, K. Zhang, B. Li, C. Yuan, Y. Zou, Z. Wang, H. Peng, *Mater. Today Nano* **2024**, *25*, 100450.
- [24] D. Y. Lu, J. Chen, J. Zhou, S. Z. Deng, N. S. Xu, J. B. Xu, *J. Raman Spectrosc.* **2007**, *38*(2), 176–180.
- [25] Z. Miao, J. Meng, M. Liang, Z. Li, Y. Zhao, F. Wang, L. Xu, J. Mu, S. Zhuo, J. Zhou, *Carbon* **2021**, *172*, 324–333.
- [26] P. Ryšánek, O. Benada, J. Tokarský, M. Syrový, P. Čapková, J. Pavlík, *Mater. Sci. Eng. C* **2019**, *105*, 110151.
- [27] N. Zhang, Y. Zhao, Y. Lu, G. Zhu, *Mater. Sci. Eng. B* **2017**, *218*, 51–58.
- [28] Z. Ying, S. Chen, S. Zhang, T. Peng, R. Li, *Appl. Catal., B* **2019**, *254*, 351–359.
- [29] Y. Huang, B. Wang, P. Liu, S. Zhao, X. Wu, S. Zhang, R. Li, Q. Jiang, F. Wang, Y. Zhao, R. Zhang, *Nano Res.* **2023**, *16*(10), 12165–12172.
- [30] Y. Wang, N. Chen, B. Zhou, X. Zhou, B. Pu, J. Bai, Q. Tang, Y. Liu, W. Yang, *Nano-Micro Lett.* **2023**, *15*(1), 231.
- [31] F. Lu, Y. Ji, D. Shi, J. Yao, L. Pei, *J. Colloid Interface Sci.* **2023**, *641*, 510–520.
- [32] A. Ramadoss, K. Y. Yoon, M. J. Kwak, S. I. Kim, S. T. Ryu, J. H. Jang, *J. Power Sources* **2017**, *337*, 159–165.
- [33] M. Beg, K. M. Alcock, A. Titus Mavelil, D. O'Rourke, D. Sun, K. Goh, L. Manjakkal, H. Yu, *ACS Appl. Mater. Interfaces* **2023**, *15*(44), 51100–51109.
- [34] X. Wang, Y. Lu, H. Zhao, Y. Sun, R. Wang, *Nanoscale* **2021**, *13*(14), 6921–6926.
- [35] A. Ramadoss, A. Mohanty, K. G. Saravanan, M. Kundu, S. Z. Noby, K. Kirubavathi, K. Selvaraju, L. S. Mende, *Ionics* **2022**, *28*(5), 2513–2524.
- [36] X. Xu, S. Chang, Z. Hong, Y. Zeng, H. Zhang, P. Li, S. Zheng, Z. Wang, S. Duo, *Nanotechnology* **2022**, *33*(5), 055402.
- [37] R. Abreu, M. Santos Klem, T. Pinheiro, J. Vaz Pinto, N. Alves, R. Martins, E. Carlos, J. Coelho, *FlatChem* **2024**, *46*, 100672.
- [38] Y. Luo, Y. Tang, X. Bin, C. Xia, W. Que, *Small* **2022**, *18*(48), 2204917.
- [39] W. Wang, H. Xu, W. Zhao, J. Zhao, M. Jiang, S. Liu, W. Huang, Q. Zhao, *Chem. Eng. J.* **2022**, *428*, 131089.

Manuscript received: August 21, 2024

Revised manuscript received: October 30, 2024

Accepted manuscript online: November 6, 2024

Version of record online: November 20, 2024